

# Towards a passive self-assembling macroscale multi-robot system

Martin Jílek\*, Michael Somr<sup>†</sup>, Miroslav Kulich\*, Jan Zeman<sup>†</sup> and Libor Přeučil\*

\*Czech Institute of Informatics, Robotics and Cybernetics  
Czech Technical University in Prague

Email: {martin.jilek.2, miroslav.kulich, libor.precuil}@cvut.cz

<sup>†</sup>Faculty of Civil Engineering

Czech Technical University in Prague

Email: michael.somr@fsv.cvut.cz, jan.zeman@cvut.cz

**Abstract**—The combined efforts of theoretical computer science, biochemistry, and nanotechnology have enabled the design of tile-based systems capable of self-assembling intricate patterns in a massively parallel manner, with low error rates, and applications ranging from DNA computing to microelectronics. However, as the underlying physical and chemical principles do not directly translate from micro to the macroscale, the transition to centimeter-scale systems remains challenging. In this contribution, we propose a framework for designing macroscale passive robots (tiles) capable of targeted self-assembly under uncontrolled external mechanical excitation. Self-assembly at this scale is achieved by using properly designed magneto-mechanical locks (glues) to accomplish jamming-free assembly, a dedicated encoding of glues to guide tile interactions, and consistent formalization of geometrical constraints that ensure the valid assembly. The potential of our framework is demonstrated by the errorless assembly of a chessboard pattern, thereby showing its robustness, three-fold increase in error recovery, and two-fold increase in growth rate, when compared to a fully magnetic approach.

## I. INTRODUCTION

Self-assembly<sup>1</sup> is a massively parallel method for bottom-up manufacturing of complex objects. *Active* self-assembly systems are controlled via assembly planning and control algorithms, e.g. [1], [2], [3]. The assembling elements are capable of changing the state of their connectors [4], [5], or they are manipulated by the environment, typically a controlled fluid flow [6], [7], [8], [9]. Thus, the process can be dynamically driven towards the formation of the target structure.

In contrast, the *passive* self-assembly requires little to no control. It is an analogy to chemical reactions, where we influence global parameters of the system (e.g., temperature), but not states of individual molecules. The commonly used self-assembly approaches include (1) the tile-based self-assembly (TBSA) proposed by Winfree [10] and (2) the DNA origami proposed by Rothmund [11]. TBSA assumes that the assembly occurs in an environment with freely moving tiles that stick together upon contact. For example, in the microscale (sub-millimeter) TBSA, where the tiles are woven from DNA, the tiles are held together with bonds between their nucleobases. As the majority of the TBSA research focuses on

<sup>1</sup>We understand self-assembly as a dissipative assembly of elements randomly moving within a perturbed environment.

microscale self-assembly, its technology has rapidly evolved over the last three decades; from the assembly of a 7 nm DNA cube [12] to assembly of a picture containing 8,704 molecular pixels arranged in an  $8 \times 8$  tile pattern [13] or implementation of tile-based molecular computation [14] with an overall error rate as low as 1 out of 3,000 tiles.

The transition from microscale to macroscale passive self-assembly (with tile size exceeding a millimeter) is not straightforward. While DNA TBSA relies on chemical bonds [10], macroscale experiments most often utilize magnetic forces, e.g., [15], [16], [17]. Moreover, the number of self-assembling tiles in DNA experiments is several orders of magnitude higher than in the macroscale case. For example, the DNA Sierpinski triangle assembly by Rothmund et al. [18] operates with hundreds of nanomoles of tiles ( $\approx 10^{16}$  tiles), whereas the analogous macroscale pattern [16] is assembled using only 14 tiles.

Although the field of macroscale passive self-assembly exists, the complexity and size of the assembled patterns are substantially lower than for the microscale ones. Majumder et al. [15] simulated a system of tiles carrying 1D magnet arrays, where pairs of tiles form bonds when subjected to excitation. Tiles with 2D arrays of magnets, proposed in our previous work, assembled  $2 \times 2$  squares and up to 7-tile long linear chains [19]. Miyashita et al. [20] proposed a system capable of assembling fragments of a chessboard correctly; however, the assembly was prone to defects. A tile system combining magnets and protrusions, making tile interactions *specific* (allowing only certain interactions), was introduced by Daiko et al. [16], and it has assembled a Sierpinski triangle containing 10 tiles without errors in 30 minutes. A similar approach was also used to assemble simple letters [17], where the specificity was achieved by a connector consisting of a 2D array of mechanical pins whose layout was optimized by a genetic algorithm. A connector design with respect to the area of acceptance from configuration space was dealt by Eckenstein and Yim [21].

The paper is structured as follows. Section II summarizes our contributions, and the theory of self-assembly is briefly introduced in Section III. Section IV describes the proposed framework of TBSA-compatible tile design along with the description of prototypes. Section V describes the validation experiment and the results we obtained, and the discussion of

the results follows in Section VI.

## II. CONTRIBUTIONS

The main goal of this paper is to contribute to macroscale self-assembly research by proposing a novel passive tile system compatible with the TBSA framework. In particular, we:

- Introduce an improved tile design featuring local interactions and jamming-free mechanical design,
- Propose a method that allows for encoding of a given set of binding interactions. We show that their number grows exponentially with a tile height,
- Formalize and utilize the geometrical constraints which a macroscale tile must respect to assemble without jamming.

Our solution is an improvement of our previous chain/square-assembling unseeded TBSA system [19] with fully magnetic connectors. The magneto-mechanical connector of the proposed system removes several drawbacks of magnetic connectors, namely their low specificity [15] and a limited number of unique connector interactions within the system. The tile design also prevents problems with jamming of tiles that use protrusions [17] to encode possible interactions.

## III. FORMAL THEORY OF TILE ASSEMBLY

The tile-based self-assembly (TBSA) process was formalized by Winfree [10] together with its elementary model—the abstract tile assembly model (aTAM), whose parameters have no direct physical meaning and that does not account for errors during assembly. Even though more advanced versions have been developed, e.g., kinetic tile assembly model [10], two-handed assembly model [22], or staged self-assembly model [23], the presented work follows the aTAM assumptions because of two reasons. First, we can benefit (especially in future work) from a large body of theory developed for the model—from proofs of the complexity of building shapes [24] to algorithms for effective design of optimal tilesets [25], [26]. Second, we use the model to establish elementary concepts, and the aTAM is a common ground for a wide range of detailed self-assembly models.

The aTAM assumes that each *tile* is a square, and each edge of a tile carries a *glue* (lock). Tiles and glues are passive and time-invariant. Glues can be of different *types* and with different *strengths*. Two glues of the same type are considered to be *matching*. Upon contact, a permanent bond is formed between two matching glues (and the tiles they belong to), and the assembly grows; however, the growth can be initiated only from a *seed assembly*. The tiles in the assembly can occupy only positions determined by a regular orthogonal grid — *binding places*, and the tiles are not allowed to rotate. The terminology is illustrated in Fig. 1.

The assembly process takes place in a *reactor* which supplies energy to the system. The driving of the system can be based upon a variety of principles, e.g., DNA assembly is commonly powered by heat [10], while macroscale experiments often utilize mechanical excitation [19], [17], [16],

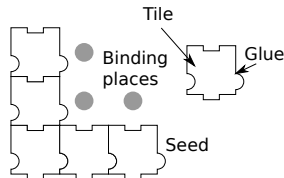


Fig. 1: Illustration of the terminology used in this work.

fans [15] or fluid turbulence [27]. The parameter expressing the amount of excitation, the *temperature*, is an integer specifying which tile aggregates will be stable and which will not. Throughout this work, we consider a reactor temperature of 2 and a glue strength of 1, *i.e.*, the tile is permanently bound to the assembly if it is connected by at least 2 matching glues.

## IV. GLUE AND TILE DESIGN

This section describes the design framework of aTAM-compatible passive macroscopic tiles. First, the design of a tile with an increased local interaction rate is described. Then, we derive formal constraints the tiles must satisfy for a jamming-free assembly. The last part proposes an efficient encoding scheme for the generation of glues.

### A. Tile and glue prototypes

We propose a novel design of macroscale 3D tiles capable of TBSA, where all the horizontal cross-sections satisfy the jamming-free conditions stated in Section IV-B. The design and assembly of the system are consistent with the aTAM philosophy. Nevertheless, as the aTAM is nonphysical, some aspects of creating a physical prototype (e.g., the extrusion to the third dimension) required a relaxation of aTAM assumptions. Each tile is a block with vertical faces carrying arrays of horizontal tongues and grooves (*shelves*), see Fig. 6, which, together with the cylindrical magnets, form glues. The tiles are composed of a lower and upper part that, after fitting together, encapsulate the magnets in the pockets, see Fig. 2a. The magnets are oriented either horizontally (in the middle of each vertical face) or vertically (in the middle of each vertical edge), as shown in Fig. 2b. The primary role of the horizontal magnets is to hold matching tiles together upon contact, while the vertical magnets lead to the formation of temporary revolute joints between tiles, similarly to the M-Block robot [28]. Thus, the tile with matching glues that is not perfectly connected at a binding place has a higher chance of binding to the assembly, as it stays in a close neighborhood of a correct tile for a longer time. Since the magnets are diametrically magnetized and free to rotate, all pairs of glues are attracted together. The specificity of tile interactions is guaranteed exclusively by the shelves. The interaction rate is further increased by the horizontal smoothness of the tiles. As there are no vertical obstacles, the tiles can smoothly slide along each other, which makes it easier not only to bind matching tiles but also to disassemble nonmatching ones. Moreover, the vertical edges are rounded with a radius of curvature of 0.9 mm to ensure a constant distance between vertical magnets in a pair of rotating tiles and to reduce their mechanical wear caused by collisions.

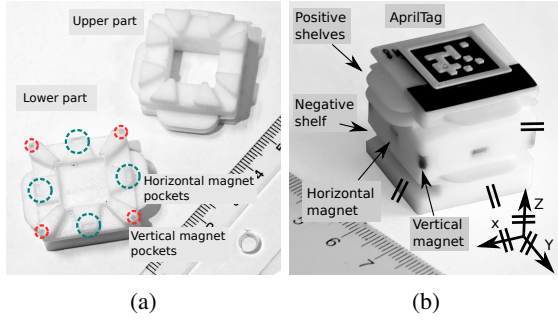


Fig. 2: Dismantled tile–magnets can be encapsulated in pockets in its faces and edges (a). The presented design of tiles with magneto-mechanical glues (b).

The tiles were manufactured using the Elegoo Mars 3D printer with a photosensitive Prusa ABS-like resin. Each tile weighs 16 g, its width is 27 mm, and its height 26 mm. The distance between magnets in neighboring tiles is 0.6 mm. Moreover, each tile carries an AprilTag [29] on its upper face to enable camera tracking and automatic analysis of experiments.

### B. Formulation of geometry constraints

To derive conditions that guarantee the jamming-free progress of the assembly, we focused exclusively on the *binding event*. The binding event is a situation when two static tiles, forming an L-shaped assembly, accommodate a third, matching tile. The experiments showed that tackling such a situation is crucial for preventing obstructions in a binding place, as illustrated in Fig. 3, which would consequently lead to a slowdown of the assembly process or even the inability to self-assemble.

Since the proposed tiles move within a 2D plane, we perform the following reasoning with 2D tiles. Observations showed that all the tiles and their binding places must satisfy two conditions, namely (1) *rotation* and (2) *translation conditions*, to bind successfully.

As we assume that the tiles are 2D entities, each tile can be considered as a set of points in a 2D plane. Let a glue on a tile edge be a 1D function  $f : D_f \rightarrow \mathbb{R}$ , where  $D_f = (0, x_{\text{tile-width}})$  and  $f(x)$  is a height of the glue on the coordinate  $x$ , see Fig. 4. When the tiles move, the functions associated with their glues also move. Therefore, we must prevent their intersection to guarantee the jamming-free motion of tiles.

1) *Rotation condition*: As shown in Fig. 4, each point  $(x_k, f(x_k))$  of a glue on a rotating tile travels along a circle defined by its center  $S = (x_c, y_c)$  and the point  $(x_k, f(x_k))$ , with an expression

$$y = \sqrt{(x - x_c)^2 + (x_k - x_c)^2 + (f(x_k) - y_c)^2} + y_c \quad (1)$$

Notice that  $x_k$  serves as a parameter that selects the point for which we calculate the trajectory.

To guarantee that a point  $(x_k, f(x_k))$  will not collide with other points, we must ensure that the circular trajectory of the

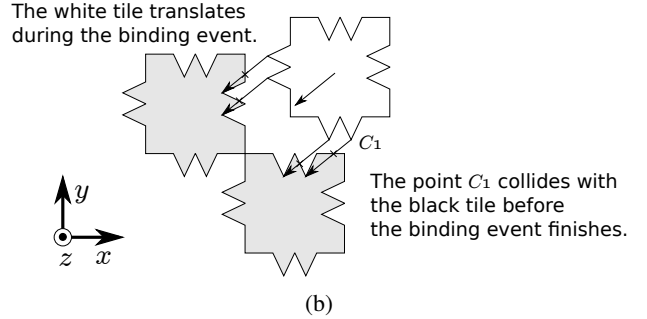
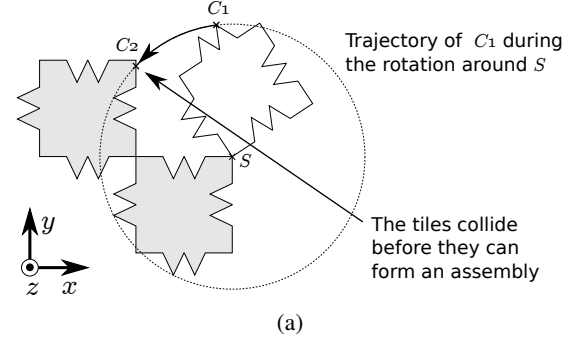


Fig. 3: Illustration of a blockage of a seed (grey tiles) by a rotating (a) and translating (b) loose tile (white)—top view.

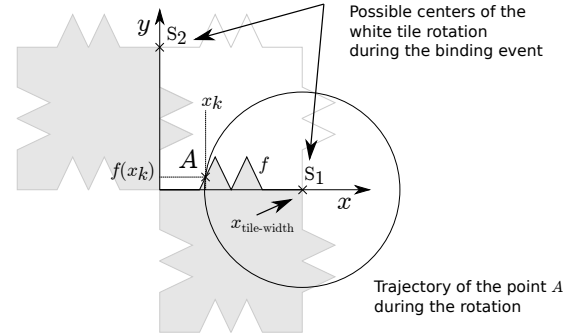


Fig. 4: Representation of a glue as a function  $f$ —top view.

point will intersect the function  $f$  only once. Thus, formally, the *rotation condition* itself states that a nonlinear equation:

$$f(x) = \sqrt{(x - x_c)^2 + (x_k - x_c)^2 + (f(x_k) - y_c)^2} + y_c \quad (2)$$

must have exactly one solution for each  $x_k \in D_f$ . Otherwise, some collisions will occur during the rotation around  $S$ . In practice, the tile rotates around  $S_1$  or  $S_2$  (as in Fig. 4) due to vertical magnets in the tile edges. Thus, the condition must be satisfied for both these centers of rotation.

2) *Translation condition*: is derived analogically and states that:

$$\frac{df(x)}{dx} \leq \left| \tan\left(\frac{\pi}{4}\right) \right| \quad \text{for all } x \in D_f \quad (3)$$

In other words, the tangent of the function  $f$  cannot have an angle larger than 45 degrees. Otherwise, there is no way for tiles to connect into the L-shaped structure. Regarding this condition, the smaller the angle, the better.

To verify that our glues satisfy the translation and rotation conditions, we split possible configurations of 3 matching tiles  $T_1, T_2, T_3$  into six horizontal cross-section (see Fig. 5a) and performed the following procedure for each of them. The verification is based on a graphical method, as depicted for the cross-section 5 in Fig. 5b. The translation condition is clearly satisfied by this slice, since  $T_2$  can freely translate from the bonded position. The satisfaction of rotation condition is verified by drawing a number of circular arcs which have centers in points  $S_1, S_2$ . Each arc  $A_i$  is a trajectory of some point  $c_i = (c_{ix}, c_{iy})$  located on a  $T_2$  glue during the (rotational) binding event. Since neither arc intersects the  $T_1, T_3$ , this particular cross-section satisfies the rotation condition.

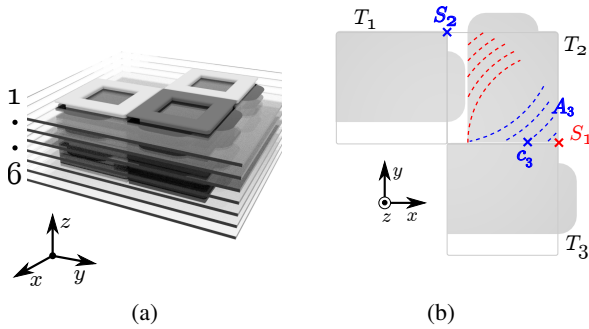


Fig. 5: (a) Illustration of horizontal cross-sections through a valid configuration of three tiles and (b) schematic of a graphical method used to verify a satisfaction of rotation and translation conditions by a cross-section 5.

### C. Glue encoding methodology

This section describes the methodology which was used to make glue interactions specific and explains how we applied the method to the design of the chessboard assembling prototype.

Each vertical face of a tile carries a glue. The type of the glue is encoded with the placement of shelves in the form of a positive shelf (tongue) or a negative shelf (groove). The shelves can occupy only discrete positions. The occupancy of the positions defines the *glue type*, as illustrated in Fig. 6.

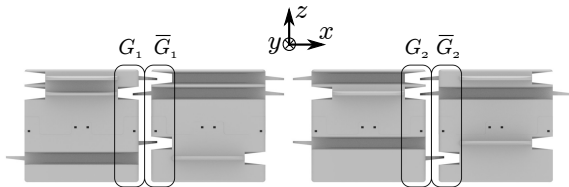


Fig. 6: Side view of matching pairs of glues  $G_i$  and  $\bar{G}_i$ .

Tongue and groove system allows for encoding of a number of glues which grows exponentially with a number of shelves the tile face can accommodate. Let a *position*  $p_i$  be a matching pair of tongue ( $p_{i+}$ ) and groove ( $p_{i-}$ ). When stacked into an array, matching pairs give rise to a *codeword* – a set of

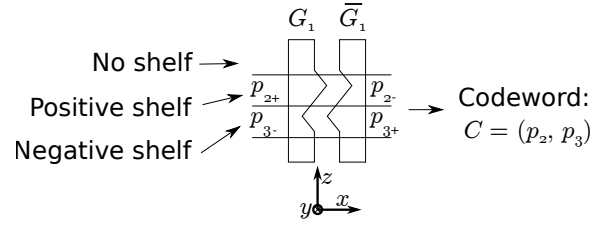


Fig. 7: Side view of schematic relationship between a pair of matching glues and a codeword which describes it.

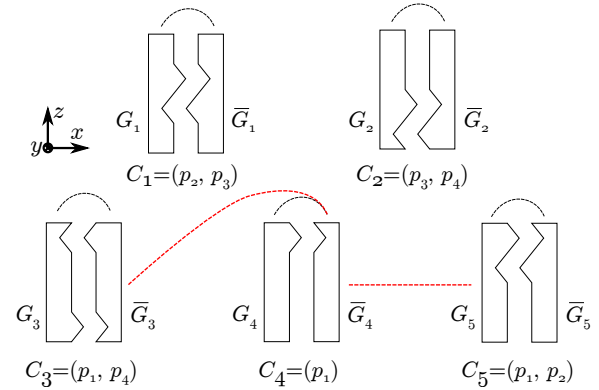


Fig. 8: Side view of matching glue pairs generated by a conflicting set of codewords  $\{C_1, C_2, C_3, C_4, C_5\}$ . Black lines connect matching glues. The red lines denote the interactions which make the set conflicting.

positions. The relationship between a pair of matching glues and a corresponding codeword is illustrated in Fig. 7.

We define a *maximal codeword* for each tile system. It is a set that contains all the positions possible within the tile system. For example, the maximal codeword of the tile system with glues in Fig. 7 is  $C_{\max} = (p_1, p_2, p_3, p_4)$ . Two codewords where one is a proper subset of the other are called *conflicting*. When no codeword is a proper subset of the other, they are *nonconflicting*. The presence of conflicting codewords in a tile system can lead to a situation when more glue types match together (i.e., glues are not sufficiently specific).

Conflicting codewords are shown in Fig. 8. The depicted set consists of five codewords,  $\{C_1, C_2, C_3, C_4, C_5\}$ . We can observe that the codeword  $C_4$  is a proper subset of the codewords  $C_3$  and  $C_5$ . Thus, glues generated by  $C_4$  do not only match each other, but also glues generated by  $C_3$  and  $C_5$ . This would result in a situation where one glue matches with two other glues. Removal of the codeword  $C_4$  will result in a nonconflicting set, i.e., a set of glues where each glue has only one specific counterpart.

Our goal is to find an *encoding set* of codewords—a set that does not contain any conflicting pairs. To this goal, we need to generate a set of codewords where no codeword is a proper subset of another. Thus, all the pairs of codewords in the encoding set must be of the same cardinality and they must differ by at least one element (we denote the actual number as  $l$ ). This means that the encoding set for a tile system with a maximal codeword of a cardinality  $n$  contains codewords

with cardinality  $n-l$ . There are  $n_g = \binom{n}{n-l}$  such codewords. Practically,  $n-l$  is the number of shelves present on each glue. We are interested in an encoding set with maximal cardinality

$$n_g^* = \max_{l^*} \binom{n}{n-l^*} = \max_{l^*} \binom{n}{l^*} = \binom{n}{\lceil \frac{n}{2} \rceil} \quad (4)$$

obtained with the optimal number of shelves  $l^* = \lceil \frac{n}{2} \rceil$ .

In the proposed tile system, each vertical face of a tile can be fitted with at most 6 shelves, thus,  $n = 6$ . The equation (4) says that such a tile system can utilize maximally  $\binom{6}{3} = 20$  types of matching glue pairs. Moreover, it implies that the number of matching glue pairs that can be encoded grows exponentially with the tile height.

The presented tiles are equipped with two types of codewords:  $C_1 = (p_1, p_2, p_4)$  and  $C_2 = (p_1, p_2, p_5)$ .  $C_1$  gives rise to a matching pair of glues  $G_1$  and  $\bar{G}_1$ ,  $C_2$  gives rise to  $G_2$  and  $\bar{G}_2$ . The shelves forming the glues and their interactions are depicted in Fig. 6. The glues are arranged as shown in Fig. 9; this way, each tile has only one correct orientation at its binding place.

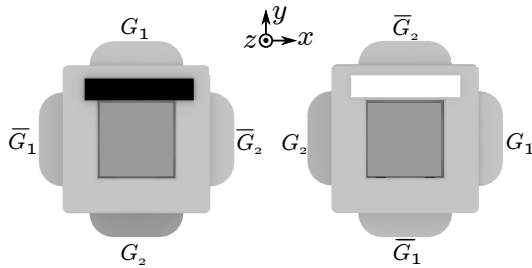


Fig. 9: Top view of black (left) and white (right) chessboard assembling tiles with their glues.  $G_1$  matches only  $\bar{G}_1$ ,  $G_2$  only  $\bar{G}_2$ .

## V. CHESSBOARD ASSEMBLY EXPERIMENT

After the design framework was established and the interaction of a few tiles was examined, we approached the experimental testing—an assembly of a chessboard pattern. This section describes conditions of our experiments, results and a comparison with a fully magnetic tile system proposed in [19].

### A. Setup

The experimental setup consists of two parts:

- Set of passive tiles consisting of 2 tile types (black and white), as illustrated in Fig. 9, where all the tiles of the same color are identical. The set contains:
  - 22 loose tiles configured for an assembly of a  $4 \times 4$  chessboard pattern, and
  - 9 fixed tiles forming an L-shaped seed,
- The reactor—a device which agitates the tiles and constrains their motion.

The reactor, see Fig. 10a, utilizes the UR5 manipulator with a custom end-effector (a platform that holds the tiles and constrains their motion onto a 2D plane) bounded by a circular barrier with a diameter of 30 cm. It agitates the tiles

by periodic elliptical motion with a constant linear velocity, as outlined in Fig. 10b. The ellipse has a semi-major axis of 3.7 cm, a semi-minor axis of 2.1 cm, and it is tilted around both  $x$ - and  $y$ -axis by 0.07 and 0.085 rad respectively.

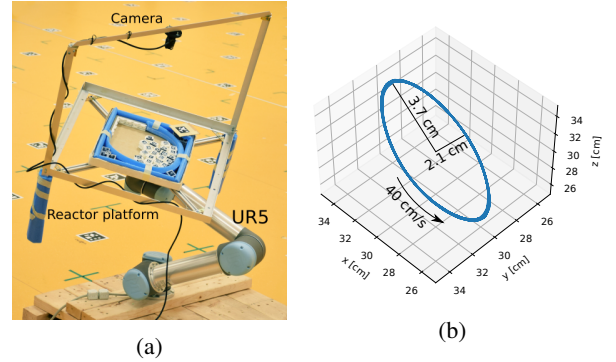


Fig. 10: (a) The reactor based on a UR5 manipulator and (b) plot of the elliptic end-effector trajectory.

The L-shaped seed assembly is fixed to the reactor plane. It is designed for the attachment of 16 tiles, limiting the resulting assembly to a chessboard pattern with a size of  $4 \times 4$  tiles. The assembly size was chosen as optimal with respect to load-bearing capacity of the seed. The plane is slightly tilted to make the tiles always slide towards the seed. All runs started from a random placement of tiles and were stopped (1) when the  $4 \times 4$  errorless chessboard was assembled or (2) when it was empirically obvious that the condition (1) cannot be fulfilled in a reasonable time (e.g., tiles were stuck in a corner).

### B. Data processing pipeline

The basis for quantitative analysis was the assembly size and the number of errors. An *error* is defined as an incorrectly placed (or oriented) tile that is bound to the seed assembly. *Assembly size* is the number of tiles in an assembly growing from the seed (including errors).

The videos captured through experimentation were processed by a combination of automatic and manual methods. The automatic pipeline detects AprilTags on the top of tiles and compares the tile positions with the given target assembly for each frame. All tiles outside the  $4 \times 4$  target pattern are neglected. A seed assembly is detected via a connected component analysis. Its size is recorded as the assembly size and all errors in the seed assembly are counted.

The resulting time series of assembly sizes and errors are filtered with a median filter with a window of 5 frames, which corresponds to 1.25 s and approximately 2 periods of the reactor cycle.

### C. Results

The data from 27 experimental runs were processed with the pipeline described above. We were interested in (1) the evolution of assembly in individual runs, (2) rate of growth, and (3) the self-repair capability.

First, a qualitative analysis of assembly progress was performed. We identified 3 main classes of possible experimental

outcomes, as depicted in Fig. 12: (1) monotonous growth (12 out of 27 runs), (2) non-monotonous growth (13 out of 27 runs), and (3) unfinished growth (2 out of 27 runs resulted in an assembly of size 15). Snapshots from a successful run are depicted in Fig. 11. We calculated two quantitative metrics of the assembly process. First, we analyzed the *growth time*  $t_{gN}$  – the duration from the start of the run to reaching the errorless assembly of size  $N$ . We measured  $t_{gN}$  for each run  $N \in \{1, 2, \dots, 16\}$ . The results are depicted in Fig. 13.

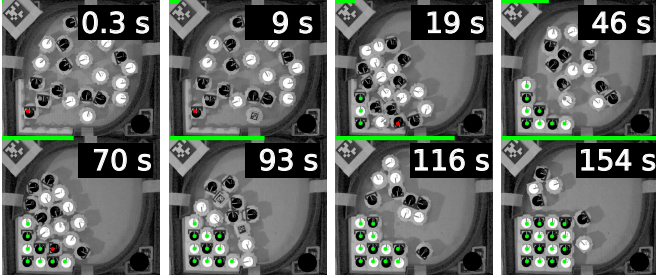


Fig. 11: Snapshots of the assembly process from a successful run. The solid green bars in the upper parts of the figures denote a fraction of the whole run which has already been completed.

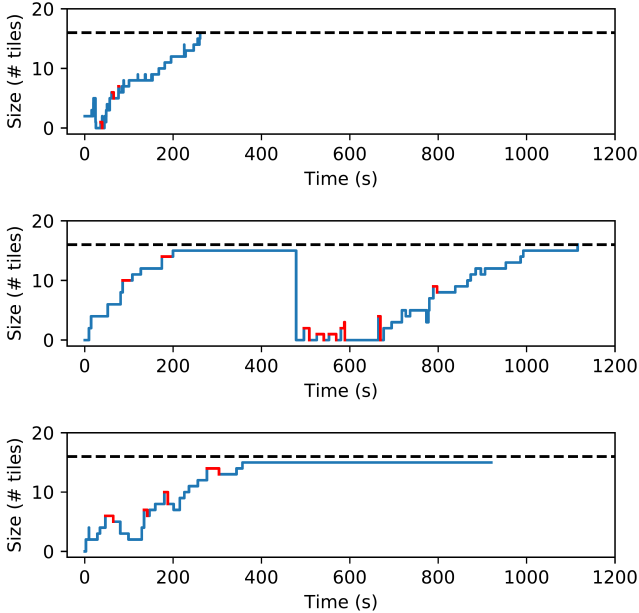


Fig. 12: Three main classes of assembly growth we observed: monotonous (top), non-monotonous (middle), and unfinished growth (bottom). The dashed line marks the size of the target assembly (16 tiles) and the red parts of a graph represent occurrence of an error.

Second, we focused on the error rate. Although the experiment confirmed that the proposed design is robust and the final assemblies contained no imperfections, some temporary errors still occur during the assembly. Since the properties of the presented system ensure a self-repair capability, errors lead to a significant slowdown of the assembly and dismantling

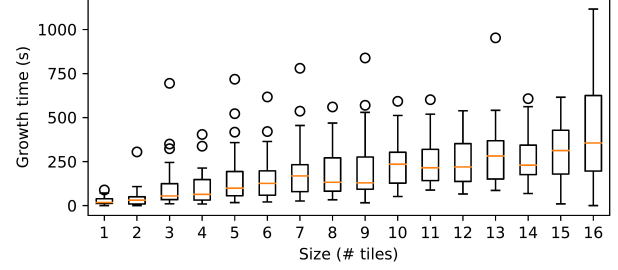


Fig. 13: Boxplots of growth times. Boxes denote the median and interquartile ranges, whiskers denote minimum and maximum observations excluding outliers (circles).

of the clusters containing them. We quantified the self-repair capability with the *recovery time*  $t_r$  – a duration in which an assembly removes all its errors. We calculated 50%, 90% and 95% percentiles of  $t_r$  and  $t_{gN}$  and summarized the results in Table I. It shows that 90% of errors are recovered in less than 41 s. We can also observe that the assembly slows down significantly after reaching a size of 15.

TABLE I: Summary of the system performance. Percentiles  $q_{p50}$ ,  $q_{p90}$ , and  $q_{p95}$  are calculated over all the captured data.

Metric	$q_{p50}$	$q_{p90}$	$q_{p95}$
Recovery time $t_r$	7.1 s	41 s	74 s
Growth time (size 16) $t_{g16}$	356 s	820 s	1077 s
Growth time (size 15) $t_{g15}$	313 s	557 s	580 s
Growth time (size 7) $t_{g7}$	168 s	447 s	528 s

Unlike the reaction rates, as proposed by, e.g., Napp et al. [30], the error rate and growth time does not give an insight into individual reaction steps. However, calculation of these metrics requires less observations than for the reaction rates while still being comparable to other state-of-the-art literature [31], [16], [3].

#### D. Comparison with the fully magnetic self-assembly system

We compared the results with the macroscale passive TBASA system proposed in our previous work [19]. The glues were encoded using 2D arrays of permanent magnets only. The specificity of glue interactions was programmed by the placement (and orientation) of the magnets.

The fully magnetic system was used to assemble a chessboard pattern with a seed of size  $6 \times 6$ . The number of loose tiles in the reactor was 18. Our results show that, unlike the presented system, the fully magnetic system was not able to assemble a chessboard at all, despite the relatively long duration of runs (up to 2,500 s). The largest errorless assembly reached by the fully magnetic tile system contained 10 tiles. The statistical analysis of growth times was not possible for assemblies containing more than 7 tiles because of their scarce occurrence. 95% percentiles ( $q_{m95}$ ) of observed growth and recovery times are summarized in Table II, along with a speedup ( $\frac{q_{p95}}{q_{m95}}$ ) that compares the results of the fully magnetic with the proposed system.

TABLE II: Performance of a fully magnetic system [19] and speedup of the presented system during the chessboard pattern assembly.

Metric	$q_{m95}$	Speedup
Recovery time $t_r$	223 s	301 %
Growth time (size 7) $t_{g7}$	953 s	180 %
Growth time (size 16) $t_{g16}$	Not reached	-

Both the recovery and growth time are substantially shorter for the proposed tile system. Fig. 14 shows the ranges between a minimum and maximum error observed for different sizes of assemblies for both tile systems during all the runs. The maximum number of errors in assembly of the proposed system decreases to zero with increasing assembly size, while both the maximum and the minimum number of errors of the fully magnetic system converge to nonzero constants.

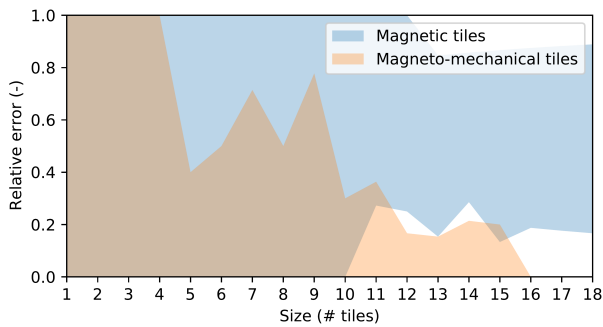


Fig. 14: Comparison of ranges of relative errors observed in different sizes of assemblies. The relative error is a ratio of number of errors and size of assembly.

## VI. CONCLUSION

We proposed and verified a novel macroscale passive robotic swarm capable of 2D self-assembly following the abstract tile assembly model (aTAM) principles. The individual robots (tiles) are entirely passive, and the assembly is driven only by an uncontrolled cyclic mechanical excitation.

Along with the realization of the prototype, we developed a suitable design framework. In particular, we formalized geometrical constraints on the shape of tiles, which, when satisfied, guarantee the jamming-free assembly of matching tiles. We also proposed and implemented a framework that generates an exponential number of glues within a linear physical space. Moreover, the generated glues are highly specific and guarantee a robust error recovery. The tile design also enables a smooth sliding of the tiles along each other, despite their protrusions. This makes it easier not only to bind matching tiles, but also to disassemble nonmatching ones.

The physical prototype demonstrated the functionality of the proposed framework during the assembly of a  $4 \times 4$  chessboard pattern. All 27 runs ended up with an errorless assembly. Two of these runs were stopped reaching an assembly consisting of 15 tiles, with the last remaining tile unable to connect. The experiments also confirmed error recovery

capability. We compared the presented results and the results obtained with a fully magnetic TBSA system [19], revealing that the proposed system has 3 times faster error recovery and almost 2 times faster growth.

## VII. FUTURE WORK

The presented system can encode up to 20 glue types; therefore, our future work will aim at the assembly of non-periodic patterns consisting of more tile and glue types. This will probably lead to a decrease of an assembly rate, since the higher number of tiles and glues might lead to a lower probability of a tile binding to a seed. Furthermore, the lower seed-binding probability might make an undesired out-of-seed assembly more favorable. We will also study how to increase the maximum size of assembly, and the influence of excitation patterns and local interactions between edge magnets on the reaction progress. The collected data will be used to create a probabilistic model of the process.

## ACKNOWLEDGMENT

The research leading to these results has received funding from the Czech Science Foundation (GAČR) under grant agreement no. 19-26143X. The work of Miroslav Kulich has been supported by the European Regional Development Fund under the project Robotics for Industry 4.0 (reg. no. CZ.02.1.01/0.0/0.0/15 003/0000470).

## REFERENCES

- [1] M. T. Tolley and H. Lipson, "On-line assembly planning for stochastically reconfigurable systems," *The International Journal of Robotics Research*, vol. 30, no. 13, pp. 1566–1584, 2011. [Online]. Available: <https://doi.org/10.1177/0278364911398160>
- [2] G. Mermoud, M. Mastrangeli, U. Upadhyay, and A. Martinoli, "Real-time automated modeling and control of self-assembling systems," in *2012 IEEE International Conference on Robotics and Automation*, 2012, pp. 4266–4273.
- [3] B. Haghghat, B. Platterier, L. Waegeli, and A. Martinoli, "Synthesizing rulesets for programmable robotic self-assembly: A case study using floating miniaturized robots," in *Swarm Intelligence*, M. Dorigo, M. Birattari, X. Li, M. López-Ibáñez, K. Ohkura, C. Pinciroli, and T. Stützle, Eds. Cham: Springer International Publishing, 2016, pp. 197–209.
- [4] B. Haghghat and A. Martinoli, "Characterization and validation of a novel robotic system for fluid-mediated programmable stochastic self-assembly," in *2016 IEEE/RSJ International Conference on Intelligent Robots and Systems (IROS)*, 2016, pp. 2778–2783.
- [5] K. Gilpin, "Shape formation by self-disassembly in programmable matter systems," PhD. thesis, Massachusetts Institute of Technology, 2012.
- [6] M. T. Tolley and H. Lipson, "Programmable 3D Stochastic Fluidic Assembly of cm-scale modules," in *2011 IEEE/RSJ International Conference on Intelligent Robots and Systems*. IEEE, Sept. 2011, pp. 4366–4371.
- [7] M. Mastrangeli, F. Schill, J. Goldowsky, H. Knapp, J. Brugger, and A. Martinoli, "Automated real-time control of fluidic self-assembly of microparticles," in *2014 IEEE International Conference on Robotics and Automation (ICRA)*, 2014, pp. 5860–5865.
- [8] M. T. Tolley, M. Krishnan, D. Erickson, and H. Lipson, "Dynamically programmable fluidic assembly," *Applied Physics Letters*, vol. 93, no. 25, p. 254105, 2008. [Online]. Available: <https://doi.org/10.1063/1.3048562>
- [9] M. T. Tolley and H. Lipson, "Fluidic manipulation for scalable stochastic 3d assembly of modular robots," in *2010 IEEE International Conference on Robotics and Automation*, 2010, pp. 2473–2478.
- [10] E. Winfree, "Algorithmic self-assembly of DNA," PhD. thesis, California Institute of Technology, 1998. [Online]. Available: <https://thesis.library.caltech.edu/1866/>

- [11] P. W. K. Rothemund, "Folding DNA to create nanoscale shapes and patterns," *Nature*, vol. 440, no. 7082, pp. 297–302, Mar 2006. [Online]. Available: <https://doi.org/10.1038/nature04586>
- [12] J. Chen and N. C. Seeman, "Synthesis from DNA of a molecule with the connectivity of a cube," *Nature*, vol. 350, no. 6319, pp. 631–633, Apr 1991. [Online]. Available: <https://doi.org/10.1038/350631a0>
- [13] G. Tikhomirov, P. Petersen, and L. Qian, "Fractal assembly of micrometre-scale DNA origami arrays with arbitrary patterns," *Nature*, vol. 552, no. 7683, pp. 67–71, Dec 2017. [Online]. Available: <https://doi.org/10.1038/nature24655>
- [14] D. Woods, D. Doty, C. Myhrvold, J. Hui, F. Zhou, P. Yin, and E. Winfree, "Diverse and robust molecular algorithms using reprogrammable DNA self-assembly," *Nature*, vol. 567, no. 7748, pp. 366–372, Mar 2019. [Online]. Available: <https://doi.org/10.1038/s41586-019-1014-9>
- [15] U. Majumder and J. H. Reif, "A framework for designing novel magnetic tiles capable of complex self-assemblies," in *Unconventional Computing*. Berlin, Heidelberg: Springer Berlin Heidelberg, 2008, pp. 129–145. [Online]. Available: [http://link.springer.com/10.1007/978-3-540-85194-3\\_12](http://link.springer.com/10.1007/978-3-540-85194-3_12)
- [16] T. Daiko and M. Satoshi, "Multistate part for mesoscale self-assembly," in *SICE Annual Conference 2007*, Sept. 2007, pp. 890–895. [Online]. Available: <http://ieeexplore.ieee.org/document/4421110/>
- [17] A. Masumori and H. Tanaka, "Morphological computation on two dimensional self-assembly system," in *ACM SIGGRAPH 2013 Posters*, ser. SIGGRAPH '13. New York, New York, USA: ACM Press, 2013.
- [18] P. W. K. Rothemund, N. Papadakis, and E. Winfree, "Algorithmic self-assembly of DNA sierpinski triangles," *PLOS Biology*, vol. 2, no. 12, 12 2004. [Online]. Available: <https://doi.org/10.1371/journal.pbio.0020424>
- [19] M. Jilek, M. Kulich, and L. Pfeučil, "Centimeter-scaled self-assembly: A preliminary study," in *Proceedings of the 17th International Conference on Informatics in Control, Automation and Robotics - ICINCO*. SciTePress, 2020, pp. 438–445.
- [20] S. Miyashita, Z. Nagy, B. Nelson, and R. Pfeifer, "The influence of shape on parallel self-assembly," *Entropy*, vol. 11, no. 4, pp. 643–666, Oct. 2009. [Online]. Available: <http://www.mdpi.com/1099-4300/11/4/643>
- [21] N. Eckenstein and M. Yim, "Modular robot connector area of acceptance from configuration space obstacles," in *2017 IEEE/RSJ International Conference on Intelligent Robots and Systems (IROS)*, 2017, pp. 3550–3555.
- [22] E. D. Demaine, M. J. Patitz, T. A. Rogers, R. T. Schweller, S. M. Summers, and D. Woods, "The two-handed tile assembly model is not intrinsically universal," in *Automata, Languages, and Programming*, F. V. Fomin, R. Freivalds, M. Kwiatkowska, and D. Peleg, Eds. Berlin, Heidelberg: Springer Berlin Heidelberg, 2013, pp. 400–412.
- [23] C. Chalk, E. Martinez, R. Schweller, L. Vega, A. Winslow, and T. Wylie, "Optimal Staged Self-Assembly of General Shapes," *Algorithmica*, vol. 80, no. 4, pp. 1383–1409, Apr. 2018. [Online]. Available: <http://link.springer.com/10.1007/s00453-017-0318-0>
- [24] D. Soloveichik and E. Winfree, "Complexity of self-assembled shapes," in *DNA Computing*, C. Ferretti, G. Mauri, and C. Zandron, Eds. Berlin, Heidelberg: Springer Berlin Heidelberg, 2005, pp. 344–354.
- [25] X. Ma and F. Lombardi, "Synthesis of tile sets for DNA self-assembly," *IEEE Transactions on Computer-Aided Design of Integrated Circuits and Systems*, vol. 27, no. 5, pp. 963–967, 2008.
- [26] M. Göös, T. Lempäinen, E. Czeizler, and P. Orponen, "Search methods for tile sets in patterned DNA self-assembly," *Journal of Computer and System Sciences*, vol. 80, no. 1, pp. 297 – 319, 2014. [Online]. Available: <http://www.sciencedirect.com/science/article/pii/S0022000013001499>
- [27] P. Löthman, "Macroscopic magnetic self assembly," PhD. thesis, University of Twente, Netherlands, Mar. 2018.
- [28] J. W. Romanishin, K. Gilpin, S. Claiici, and D. Rus, "3D M-Blocks: Self-reconfiguring robots capable of locomotion via pivoting in three dimensions," in *2015 IEEE International Conference on Robotics and Automation (ICRA)*, May 2015, pp. 1925–1932, iSSN: 1050-4729.
- [29] J. Wang and E. Olson, "AprilTag 2: Efficient and robust fiducial detection," in *Proceedings of the IEEE/RSJ International Conference on Intelligent Robots and Systems (IROS)*, October 2016.
- [30] N. Napp, S. Burden, and E. Klavins, "The statistical dynamics of programmed self-assembly," in *Proceedings 2006 IEEE International Conference on Robotics and Automation, 2006. ICRA 2006.*, 2006, pp. 1469–1476.
- [31] P. White, V. Zykov, J. Bongard, and H. Lipson, "Three dimensional stochastic reconfiguration of modular robots," in *Robotics: Science and Systems I. Robotics: Science and Systems Foundation*, 2005. [Online]. Available: <https://doi.org/10.15607%2Frss.2005.i.022>